

# Three-dimensional particle-in-cell modeling of parametric instabilities near the quarter-critical density in plasmas

H. Wen<sup>1,2,\*</sup>, A. V. Maximov<sup>1,2</sup>, R. Yan<sup>1,2,†</sup>, J. Li<sup>1,2,‡</sup>, C. Ren<sup>1,2,3</sup>, and F. S. Tsung<sup>4</sup>

<sup>1</sup>Laboratory for Laser Energetics, University of Rochester, Rochester, New York 14623-1299, USA

<sup>2</sup>Department of Mechanical Engineering, University of Rochester, Rochester, New York 14627, USA

<sup>3</sup>Department of Physics and Astronomy, University of Rochester, Rochester, New York 14627, USA and

<sup>4</sup>Department of Physics and Astronomy, University of California Los Angeles, Los Angeles, California 90095, USA

(Dated: July 19, 2022)

The interplay between two-plasmon-decay (TPD) and stimulated Raman scattering (SRS) instabilities has been studied in three-dimensional particle-in-cell simulations with parameters relevant to the inertial confinement fusion experiments. SRS and TPD develop in the same region in plasmas, and the generation of hot electrons can be described accurately with only the full model including both SRS and TPD. The growth of instabilities in the linear stage is found to be in good agreement with analytical theories. In the saturation stage the Langmuir-decay instability driven by the daughter waves of the SRS sidescattering can saturate the TPD and consequently inhibit the hot-electron generation.

Since the 1960s, the pursuit of inertial confinement fusion (ICF) driven by lasers has led to large-scale research on laser interaction with the plasmas of ICF targets [1]. Decades of laser-plasma interaction (LPI) research [2] have concentrated on several processes in laser-produced plasmas that can grow as parametric instabilities at high-enough laser intensities, namely stimulated Raman scattering (SRS), stimulated Brillouin scattering (SBS), and two-plasmon decay (TPD). The evolution of SRS, SBS, and TPD strongly influences the balance between absorption and scattering of laser light in ICF plasmas.

Laser light can propagate in a plasma up to the critical density determined by the laser frequency. SRS can develop only at densities up to the quarter-critical density, and TPD can develop near the quarter-critical density, which makes the region near quarter-critical density a possible place for the interplay between SRS, SBS, and TPD. SRS and TPD produce plasmons that can generate hot electrons, and hot electrons from LPI instabilities are a concern in ICF experiments since they can move to the target center, deposit their kinetic energy into the fusion fuel, cause the fuel to preheat and degrade the performance of the ICF targets [1]. Several mechanisms of fast-electron acceleration have been studied before, namely staged acceleration [3], Langmuir cavitation [4, 5], and wave breaking [6].

In this Letter, LPI is studied using particle-in-cell (PIC) modeling [7], which can describe the interplay between different plasma instabilities and also the particle distributions including hot-electron generation. Two-dimensional (2-D) PIC studies have been performed in the past [3]. Usually, few hot electrons are found in the simulations at the linear stage of the TPD and SRS instabilities. The electron acceleration becomes effective after the instabilities saturate [3].

The TPD-related waves are mostly localized in the plane of polarization [8], which is defined by the incident laser wave vector (in the  $x$  direction) and the laser elec-

tric field vector (in the  $y$  direction). The SRS sidescattering (SRSS) develops mostly outside of the polarization plane, and its scattered-light wave vector is almost perpendicular to the incident laser wave vector [9, 10]. Scattered light waves can also propagate in the direction parallel or anti-parallel to the laser wave vector (forward and backscattering, respectively) [11]. A 2-D simulation in the polarization plane ( $x$ - $y$ ) or in the perpendicular plane ( $x$ - $z$ ) will be referred to as  $p$  polarized (PP) or  $s$  polarized (SP), respectively. Two-dimensional simulations can model only the interaction where either TPD or SRS dominates except for the case when the SRS scattered light propagates in the backward direction and the SRS-related and TPD-related waves are in the same ( $x$ - $y$ ) plane [this instability is known as high-frequency hybrid instability (HFHI) [12]]. The 3-D simulations are required to study the interaction including both TPD and SRS. In this Letter, the results of several 3-D simulations for different plasma parameters and incident laser profiles are presented and compared with the respective 2-D simulations to illustrate that the TPD and SRS can co-exist near quarter-critical density and the interplay of these instabilities can lead to different energy distributions of hot electrons.

Here we describe in detail a 3-D simulation for the parameters relevant to ICF experiments [13]. A CH plasma is initialized with the electron temperature  $T_e = 2$  keV, and the temperatures for both ion species  $T_i = 1$  keV. The incident laser beam with intensity  $I = 9 \times 10^{14}$  W/cm<sup>2</sup> propagates in the direction of density inhomogeneity ( $x$ ) and is polarized in the transverse direction ( $y$ ). A linear density profile with the scale length  $L = 100$   $\mu$ m is assumed at the initial time. The size of the simulation box is 21  $\mu$ m  $\times$  8.4  $\mu$ m  $\times$  6.7  $\mu$ m modeling the density range from 0.21  $n_c$  to 0.26  $n_c$  ( $n_c$  is the critical density).

Two 2-D simulations (PP and SP) with the same physical parameters were also performed. The PP simula-

tion models mostly the TPD instability and the SP simulation models mostly the SRS instability. The TPD threshold parameter  $\eta$  [8] is 1.9 ( $\eta = 1$  at threshold), and the SRS backscattering threshold parameter  $N$  [11] is 0.5 ( $N = 0.26$  at SRS threshold) for these simulations. The SRSS threshold [9, 10] is close to the SRS backscattering threshold for these parameters, and both absolute TPD and absolute SRS instabilities are expected to grow. The threshold of the convective SRS [9] is not exceeded for the parameters described above. The time evolution of the energy of the field components in the simulation region is shown in Fig. 1. The field energy is defined as the square of the electric- or magnetic-field amplitudes integrated over the simulation region normalized to the respective laser field energy at early time (when there are no instabilities). In the 2-D PP simulation [Fig. 1(a)], the  $E_x$  field [red line in Fig. 1(a)] is associated with plasma waves propagating in the  $x$  direction, which contain most of the energy of the TPD plasmons with a larger wave vector [see the diagram in Fig. 1(c)]. One can see that the field energy associated with the TPD instability stays at about the same level (close to 70% of the energy of the incident laser electric field) after 2.5 ps, when one can assume that the saturation stage is reached. In the 2-D SP simulation, the energy of the  $B_x$  field [Fig. 1(b)] is used as an indicator for the level of SRSS instability. The energy of the scattered light saturates at a level of about 8% of the energy of the incident laser magnetic field.

In the 3-D simulation, the diagram for TPD and SRS is shown in Fig. 1(c), where the incident light ( $\vec{k}_0$ ) decays into a plasmon ( $\vec{k}_{\text{SRS},1}$ ) and a light wave ( $\vec{k}_{\text{SRS},2}$ ) in the case of SRS and into two plasmons ( $\vec{k}_{\text{TPD},1}$  and  $\vec{k}_{\text{TPD},2}$ ) in the case of TPD. The  $E_x$  field energy [red line in Fig. 1(d)] now includes the energy of the TPD plasmons with a larger wave vector and the SRS plasmons. The red line is overlaid with the dotted black line that represents the maximum TPD growth rate [8] ( $7.7 \times 10^{-4} \omega_0$ ) minus the damping rate of plasma waves ( $2.1 \times 10^{-4} \omega_0$ ) measured in the 3-D simulation. The  $E_x$  field saturates at a level of about 40% of the laser field energy, which is much lower than the saturation level in the 2-D PP simulation. The  $E_y$  field energy [blue line in Fig. 1(d)] is the sum of the energy of TPD plasmons and the energy of the electric components of the incident laser light and the SRS scattered light. The  $E_y$  field energy level remains stable for the entire simulation. The green line in Fig. 1(d) corresponds to the energy of the scattered light wave (propagating in the  $z$  direction) from the SRSS and is overlaid with the dashed purple line representing the maximum growth rate of the SRSS [9] ( $8.2 \times 10^{-4} \omega_0$ ) minus the damping rate of the plasma waves. One can see from Fig. 1(d) that the growth of the  $B_x$  field energy in time is in reasonable agreement with the theoretical result [9]. The  $B_x$  field energy is under 10% of the incident laser field energy after reaching its peak value, which is

consistent with the 2-D SP simulation result.

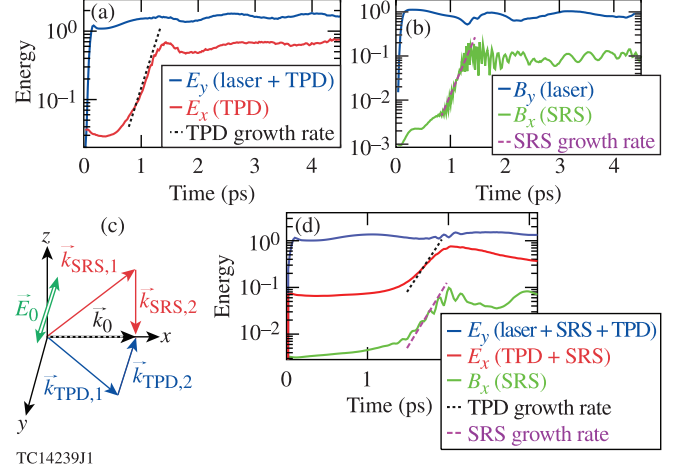


FIG. 1. The integrated energy of different field components in the simulation region as a function of time for the (a) 2-D  $p$ -polarized simulation, (b) 2-D  $s$ -polarized simulation, and (d) 3-D simulation. The wave-vector diagram for TPD and SRSS is shown in (c).

Figure 2 shows the intensities of the plasma waves ( $|\vec{E}_L|$ ) in the 2-D and 3-D simulations as a function of frequency and plasma density at the linear instability stage. The spectra of plasma waves obtained at a time interval between 0.3 ps and 1.0 ps in the 2-D PP and SP simulations are plotted in Figs. 2(a) and 2(b), respectively. From the 3-D simulation, the spectra of plasma waves at a time interval between 1.3 ps and 2.0 ps are plotted in Fig. 2(c) (close to  $k_z = 0$  plane, where TPD dominates) and in Fig. 2(d) (far away from  $k_z = 0$  plane, where SRS dominates). One can see from Figs. 2(c) and 2(d) that TPD and SRS co-exist near the quarter-critical density. The spectra of the unstable modes for TPD and SRS are close to the linear theory results (see overlaid lines in Fig. 2). Compared to the 2-D PP simulation, the frequency of the plasmons in the 3-D simulation can be lower than the frequency of TPD plasmons because SRS plasmons have lower frequencies.

As the instability evolves from the linear stage to the saturation stage, the frequency spectra shown in Fig. 2 evolve into the spectra shown in Fig. 3. Figures 3(a) and 3(b) show the plasma-wave spectra at a time interval between 3.3 ps and 4.1 ps in the 2-D PP and SP simulations, respectively. The spectra in the 3-D simulation at a time interval between 2.3 ps and 3.1 ps are shown in Figs. 3(c) and 3(d). Figure 3 illustrates that the spectra in all these simulations are broader in the saturation stage compared to the linear stage. The density in Fig. 3 is calculated using the initial density profile. As the instabilities grow, the background density changes as a result of the background relaxation and the ion perturbations driven by the instabilities. Compared to the 2-D PP simulation [Fig. 3(a)], the TPD is much weaker at densities

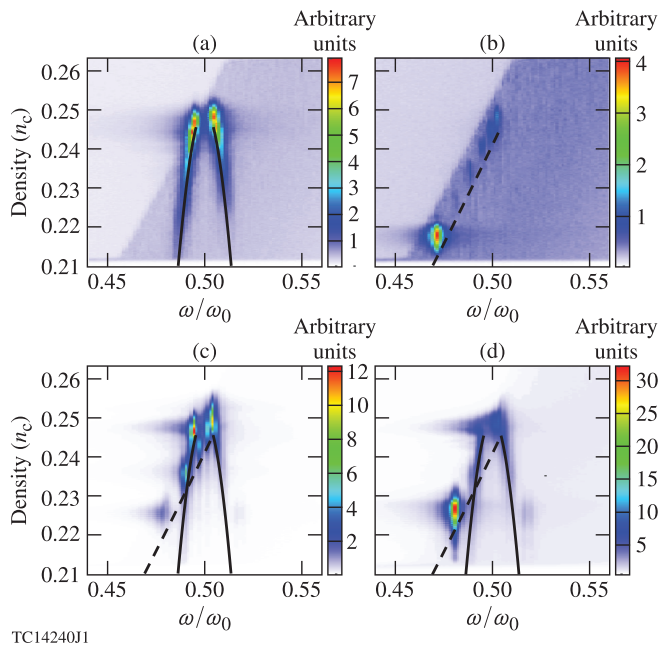


FIG. 2. (a) Plasma-wave spectra in the linear instability stage as a function of plasma density and the wave frequency normalized to laser frequency in the 2-D PP simulation, (b) 2-D SP simulation, and (c) 3-D simulation for modes with  $0 < k_z/k_0 < 0.2$  and (d)  $0.2 < k_z/k_0 < 3$ . The overlaid solid black lines and the dashed black lines represent the dispersion relations satisfying the matching conditions for TPD and SRS, respectively.

lower than  $0.23 n_c$  in the 3-D simulation [Fig. 3(c)]. The absence of the TPD modes at these densities is also illustrated in Fig. 4(a), where the spectrum of plasma waves at densities below  $0.23 n_c$  in the saturation stage is integrated over  $k_z$  and plotted in the  $k_x-k_y$  plane. There are no prominent modes along the TPD hyperbola [14] [black solid line in Fig. 4(a)] at  $k_x > k_0$ , which corresponds to the TPD daughter waves with larger wave vectors. The Langmuir-decay instability (LDI) [15] is considered to be one of the mechanisms for TPD and SRS saturation [16]. The crest-shaped feature at  $k_x \approx -0.9k_0$  in Fig. 4(a) corresponds to LDI-driven plasma waves. The LDI modes are also visible in the spectrum of the ion density fluctuations shown in Fig. 4(b). The ion density fluctuation  $\delta n$  is defined as  $\delta n = n_i - n_0$ , where  $n_i$  is the ion density and  $n_0$  is the background density obtained by averaging  $n_i$  over the transverse directions. The broad feature at  $k_x \approx 1.7k_0$  (about  $2\times$  the laser wave vector in plasma) corresponds to the ion waves from LDI. The SRS plasmons can drive stronger LDI compared to the TPD plasmons because the SRS plasmons correspond to a narrower  $k$ -space domain and therefore their  $k$ -space amplitudes are larger. The saturation of TPD due to ion density fluctuations has been reported in previous PIC simulations [17]. The correlation between the ion density perturbation and the SRSS daughter wave is clearly

shown in Fig. 4(c). Ion density fluctuations as large as 4% of the background density are observed at densities lower than  $0.23 n_c$ , which is consistent with the density range where the TPD modes are reduced but the SRSS modes are dominant. The coexistence of TPD and SRSS can be properly modeled only in the 3-D simulations. The interaction of the TPD and the SRSS can lead to a lower TPD saturation level in the 3-D simulation compared to the 2-D PP simulation, which is consistent with Fig. 1.

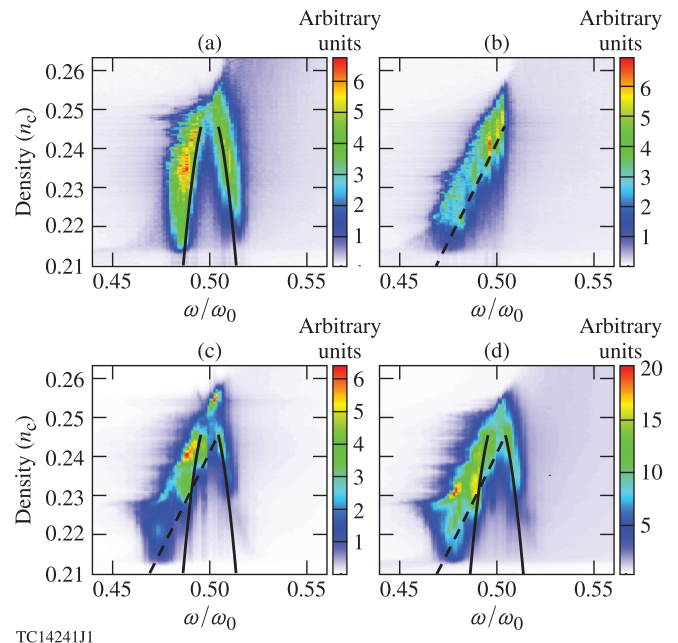
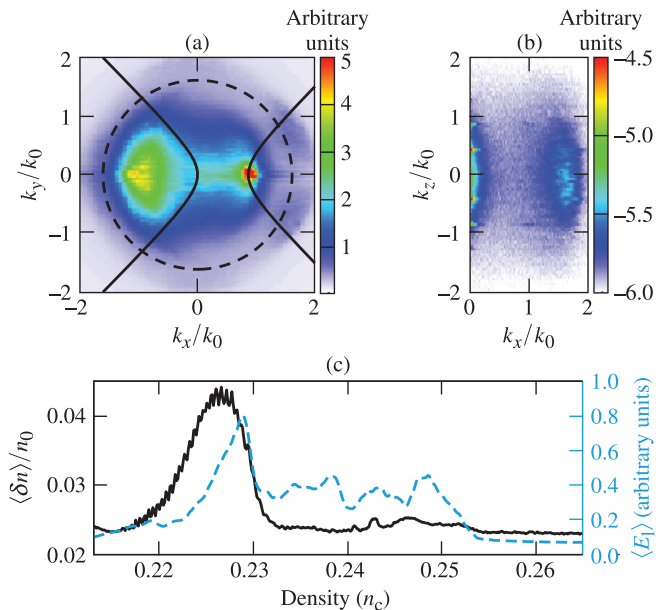


FIG. 3. Plasma-wave spectra in the saturation stage in the 2-D and 3-D simulations as a function of plasma density and the wave frequency. Each panel displays the same quantity as in Fig. 2 for the linear stage.

To characterize the energy transfer to hot electrons in PIC simulations, the hot-electron flux is defined as the energy flux carried by electrons with kinetic energy above 55 keV leaving the simulation box minus the energy flux carried by the thermal electrons injected into the simulation region from the thermal boundaries (in the  $x$  direction). Information about the hot electrons is collected during the saturation stage in each simulation for 0.5 ps. In the 3-D simulation, the hot-electron flux associated with the forward- and backward-going hot electrons was found to be 1.7% and 0.8%, respectively. The plasma-wave spectrum in the 3-D simulation corresponds to a smaller  $k$ -space domain than the spectrum in the 2-D PP simulation, which explains a smaller number of hot electrons in the 3-D simulation compared to the 2-D PP simulation (6.6% and 3.4% in the forward and backward direction, respectively).

The interactions between TPD and SRS in the saturation stage are also observed in simulations with the speck-



TC14242J1

FIG. 4. (a) The spectrum of plasmons in the saturation stage of 3-D simulation at densities lower than  $0.23 n_c$  plotted in the  $k_x$ - $k_y$  plane. The overlaid dashed circle represents the Landau cutoff condition ( $k\lambda_D \approx 0.3$ ). (b) The spectrum of ion density fluctuation plotted in the  $k_x$ - $k_z$  plane on a logarithmic scale. (c) Ion density fluctuations normalized to background density (black solid line) and longitudinal electric field (blue dashed line) as a function of the initial density. Operator  $\langle \rangle$  denotes the root-mean-square average over the transverse direction.

led laser beam [18, 19] and electron-ion collision effect included. The speckled laser beam is modeled by a single speckle in the simulation region that mirrors itself in the transverse direction because of the periodic boundary conditions. A series of simulations has been performed to study how the speckles affect the generation of hot electrons. The average intensities of the pump beam for all simulations are the same ( $9 \times 10^{14} \text{ W/cm}^2$ ) and the peak intensities in the laser speckles are  $1.8 \times 10^{15} \text{ W/cm}^2$ . The other parameters for these simulations include: the density scale length  $L = 100 \mu\text{m}$ ; the electron temperature  $T_e = 3 \text{ keV}$ ; the temperature for the carbon and hydrogen ion  $T_i = 1.5 \text{ keV}$ . A collision package (CP) is available for the PIC code OSIRIS [20] and the OSIRIS simulations have demonstrated the importance of collisional effects for the generation of hot electrons [3]. The main physics processes are observed to be the same in simulations with plane-wave beams and speckled beams.

The hot-electron flux values in simulations are listed in Table I for different incident laser beams as well as with CP turned on and off. Among all the simulations, the 3-D speckled-beam case with CP on is the closest to the real experimental conditions. By comparing the left and right columns of Table I, one can see that adding collisions can reduce the hot-electron flux by about 50% and in the case

Hot-electron flux	Forward/Backward	
Collision package	On	Off
Plane wave 2-D PP	1.6%/1.3%	5.5%/3.8%
Plane wave 2-D SP	(< 0.1%)/0.2%	(< 0.1%)/0.5%
Speckle 2-D PP	6.8%/1.7%	9.4%/3.8%
Speckle 2-D SP	(< 0.1%)/0.3%	(< 0.1%)/0.7%
Speckle 3-D	0.4%/0.3%	0.8%/0.5%

TABLE I. Hot-electron flux normalized to the incident laser energy flux.

of plane-wave 2-D PP simulation by almost 70%. Also note that the reduction of the hot-electron flux caused by collisions affects both the forward-going electrons and backward-going electrons since the collisional damping rate affects all the plasma waves. The hot-electron flux generated in the 2-D SP simulations (modeling mostly SRS) is much smaller than the hot-electron flux generated in the 2-D PP simulations (modeling mostly TPD), which indicates that the plasma waves driven by TPD are the main source of the electron acceleration. The hot-electron fraction obtained in our 3-D simulations agrees quantitatively with OMEGA experiments [21].

In this Letter the LPI in the plasma region near the quarter-critical density has been studied for conditions relevant to the ICF experiments using the PIC code OSIRIS. The net energy flux associated with the hot electrons in simulations is found to be closely related to the plasma-wave spectra. The TPD-driven plasma waves with large wave vectors are very important for accelerating electrons. At the same time, the SRS-driven plasma waves are less effective in accelerating electrons. More forward-going hot electrons are generated by the speckled beams than by the plane-wave beams. A smaller number of hot electrons are found in the 3-D simulation compared to the 2-D PP simulation. The plasma waves transfer energy to electrons through a wave-particle resonance mechanism, favoring the electrons moving in the same direction as the phase velocity of the plasma waves. It is easier for the electrons to be accelerated by the plasma waves in the 2-D simulations than in the 3-D simulations. Another reason for a smaller number of hot electrons in the 3-D simulation is that the SRS can help to saturate the TPD, especially at low densities (lower than  $0.23 n_c$ ), which breaks the “staged acceleration” [3] mechanism. Also the SRSS at low plasma densities may cause the pump depletion and reduce the laser energy reaching the higher-density region, which also leads to weaker TPD-driven plasma waves and reduces the generation of hot electrons.

This work was supported by the Department of Energy National Nuclear Security Administration under Award Number DE-NA0001944, the University of Rochester, and the New York State Energy Research and Development Authority. We also acknowledge the support by the

DOE under grant No. DE-SC0012316, and by the NSF under grant No. PHY-1314734. This report was prepared as an account of work sponsored by an agency of the U.S. Government. Neither the U.S. Government nor any agency thereof, nor any of their employees, makes any warranty, express or implied, or assumes any legal liability or responsibility for the accuracy, completeness, or usefulness of any information, apparatus, product, or process disclosed, or represents that its use would not infringe privately owned rights. Reference herein to any specific commercial product, process, or service by trade name, trademark, manufacturer, or otherwise does not necessarily constitute or imply its endorsement, recommendation, or favoring by the U.S. Government or any agency thereof. The views and opinions of authors expressed herein do not necessarily state or reflect those of the U.S. Government or any agency thereof.

---

\* Now at University of California, Los Angeles, CA 90025, USA. hanwen@ucla.edu

† Now at University of Science and Technology of China, Anhui 230026, China

‡ Now at University of California, San Diego, CA 92093, USA

- [1] R. S. Craxton, K. S. Anderson, T. R. Boehly, V. N. Goncharov, D. R. Harding, J. P. Knauer, R. L. McCrory, P. W. McKenty, D. D. Meyerhofer, J. F. Myatt *et al.*, Phys. Plasmas **22**, 110501 (2015).
- [2] J. F. Myatt, J. Zhang, R. W. Short, A. V. Maximov, W. Seka, D. H. Froula, D. H. Edgell, D. T. Michel, I. V. Igumenshchev, D. E. Hinkel, *et al.*, Phys. Plasmas **21**, 055501 (2014).
- [3] R. Yan, C. Ren, J. Li, A. V. Maximov, W. B. Mori, Z.-M. Sheng, and F. S. Tsung, Phys. Rev. Lett. **108**, 175002 (2012).
- [4] H. X. Vu, D. F. DuBois, D. A. Russell, and J. F. Myatt, Phys. Plasmas **19**, 102708 (2012).
- [5] H. X. Vu, D. F. DuBois, J. F. Myatt, and D. A. Russell, Phys. Plasmas **19**, 102703 (2012).
- [6] T. P. Coffey, Phys. Fluids **14**, 1402 (1971).
- [7] J. M. Dawson, Rev. Mod. Phys. **55**, 403 (1983).
- [8] A. Simon, R. W. Short, E. A. Williams, and T. Dewandre, Phys. Fluids **26**, 3107 (1983).
- [9] C. S. Liu, M. N. Rosenbluth, and R. B. White, Phys. Fluids **17**, 1211 (1974).
- [10] B. B. Afeyan and E. A. Williams, Phys. Plasmas **4**, 3803 (1997).
- [11] J. F. Drake and Y. C. Lee, Phys. Rev. Lett. **31**, 1197 (1973).
- [12] B. B. Afeyan and E. A. Williams, Phys. Plasmas **4**, 3845 (1997).
- [13] W. Seka, D. H. Edgell, J. F. Myatt, A. V. Maximov, R. W. Short, V. N. Goncharov, and H. A. Baldis, Phys. Plasmas **16**, 052701 (2009).
- [14] J. Meyer and Y. Zhu, Phys. Rev. Lett. **71**, 2915 (1993).
- [15] D. F. DuBois and M. V. Goldman, Phys. Rev. **164**, 207 (1967).
- [16] D. F. DuBois, H. A. Rose, and D. A. Russell, Phys. Scr. **T63**, 16 (1996).
- [17] R. Yan, A. V. Maximov, C. Ren, and F. S. Tsung, Phys. Rev. Lett. **103**, 175002 (2009).
- [18] Y. Kato, K. Mima, N. Miyanaga, S. Arinaga, Y. Kitagawa, M. Nakatsuka, and C. Yamanaka, Phys. Rev. Lett. **53**, 1057 (1984).
- [19] S. Skupsky, R. W. Short, T. Kessler, R. S. Craxton, S. Letzring, and J. M. Soures, J. Appl. Phys. **66**, 3456 (1989).
- [20] R. A. Fonseca, L. O. Silva, F. S. Tsung, V. K. Decyk, W. Lu, C. Ren, W. B. Mori, S. Deng, S. Lee, T. Katsouleas *et al.*, in *Computational Science – ICCS 2002*, edited by P. M. A. Sloot, C. J. K. Tan, J. J. Dongarra, and A. G. Goekstra, Lecture Notes in Computer Science, Vol. 2331 (Springer, Berlin, 2002) p. 342..
- [21] D. T. Michel, A. V. Maximov, R. W. Short, J. A. Delettrez, D. Edgell, S. X. Hu, I. V. Igumenshchev, J. F. Myatt, A. A. Solodov, C. Stoeckl, *et al.* Phys. Plasmas **20**, 055703 (2013).